On the Renner−Teller Effect and Barriers to Linearity and Dissociation in HCF($\tilde{A}^1A''$)

Haiyan Fan, Ionela Ionescu, Chris Annesley, Joseph Cummins, Matthew Bowers, Ju Xin,[a] and Scott A. Reid*

Department of Chemistry, Marquette University, Milwaukee, Wisconsin 53201

Received: January 13, 2004; In Final Form: February 22, 2004

To further investigate the Renner−Teller effect and barriers to linearity and dissociation in the simplest singlet carbene (HCF), we recorded fluorescence excitation spectra of the pure bending transitions 2_0^n with $n = 0-7$ and the combination bands $1_0^1 2_0^n$ with $n = 1-6$ and $2_0^n 3_0^1$ with $n = 0-3$ in the HCF $\tilde{A}^1A'' \leftarrow \tilde{X}^1A'$ system. The spectra were measured under jet-cooled conditions, using a pulsed-discharge source, and rotationally analyzed to yield precise values for the band origins and rotational constants. The derived $\tilde{A}$-state parameters are in excellent agreement with the predictions of ab initio electronic structure theory. The approach to linearity in the $\tilde{A}$ state is evidenced in a sharp increase in the rotational constant A, as first reported by Kable and co-workers, and a minimum in the vibrational intervals near the 2^7 level. A fit of the vibrational intervals for the pure bending levels yields a barrier to linearity of 6300 ± 270 cm^{-1} above the vibrationless level. Our observation of the $K_a' = 1$ level of $1^1 2^6$ places a lower limit on the $\tilde{A}$ state barrier to dissociation of ~ 8555 cm^{-1} above the vibrationless level.

Introduction

Simple carbenes are ubiquitous in chemistry; they have an important role in many organic and organometallic reactions,[1−4] in combustion[5,6] and the thermal decomposition of small organic molecules,[7−10] and in stratospheric and interstellar chemistry.[11] The electronic structure of carbenes results in low-lying singlet and triplet states with distinct chemical properties.[2,3] Electron-withdrawing substituents favor a singlet ground state,[12] and, thus, the monohalocarbenes and dihalocarbenes (HCX and CXY, respectively, where X,Y = F, Br, Cl) have singlet ground states, with the singlet−triplet gap (ΔE_{ST}) being dependent on the electron-withdrawing ability of the halogen.[13−24] As the smallest carbene with a singlet ground state, HCF is a prototype for exploring the spectroscopy, dynamics, and electronic structure of singlet carbenes.[25,26] Of particular interest is the Renner−Teller (RT) interaction between $\tilde{A}^1A''$ and $\tilde{X}^1A'$, which correlates with a $^1\Delta$ state in the linear configuration. Notably, HCF is one of a few RT molecules that exhibit a large barrier to linearity in the excited state, and because the RT interaction is maximal in the barrier region, where the wave functions overlap most strongly, HCF is an ideal system for study of the RT interaction as the barrier to linearity is approached.

The singlet−singlet emission spectra of halocarbenes such as HCF have been known in flames for many years.[27] The $\tilde{A}^1A'' \leftarrow \tilde{X}^1A'$ system was first observed in absorption by Merer and Travis,[28] who reported a progression in the bending vibration. The rotational structure exhibited severe perturbations at high J, and rotational analysis was performed only for the 2_0^1 and 0_0^0 bands. The large change in bond angle (opening by $\sim 25°$ in the excited state) led to prominent axis-switching transitions, in addition to those obeying the normal selection rules for a perpendicular transition.[28] Subsequently, Hirota and

co-workers examined the spectra of HCF and DCF under high resolution, refining the rotational constants of the 2_0^1 and 0_0^0 bands and using the Zeeman effect to probe the origin of the perturbing state(s).[29−33] The magnetic properties of $\tilde{A}^1A''$ primarily resulted from interactions with high vibrational levels of $\tilde{X}^1A'$, although localized singlet−triplet perturbations were also identified.[32,33]

Recently, Kable and co-workers reported a study of the $\tilde{A}^1A'' \leftarrow \tilde{X}^1A'$ system under jet-cooled conditions using laser-induced fluorescence (LIF).[34] The energy dependence of the rotational constant A for the pure bending levels in the $\tilde{A}^1A''$ state was determined and modeled. Excitation of the bending mode produced a dramatic increase in A, and an analysis of the vibrational intervals provided an estimate of the barrier to linearity, set between the 2^6 and 2^7 levels, in agreement with a theoretical prediction.[26]

We have recently undertaken a detailed study of the $\tilde{A}^1A'' \leftarrow \tilde{X}^1A'$ system, using fluorescence excitation spectroscopy, polarization quantum beat spectroscopy (QBS), and fluorescence lifetime measurements.[35,36] We showed that this system provides a textbook example of lifetime lengthening, in that the lifetimes of upper-state levels with $K_a' \geq 1$ display an obvious lengthening with increasing energy, because of the RT interaction.[35] Our initial polarization QBS studies of this system probed the vibrational-mode dependence of the ^{19}F and ^{1}H hyperfine interaction for the first time, and we found a striking vibrational-mode dependence of the ^{19}F spin-rotation constant C_{aa}.[36] In this article, we report our results concerning the electronic spectroscopy of the HCF $\tilde{A}^1A'' \leftarrow \tilde{X}^1A'$ system, focusing on the RT effect and excited-state barriers to linearity and dissociation.

Experimental Section

The apparatus, pulsed-discharge nozzle, and data acquisition procedures have previously been described in detail.[35−38] HCF was generated by a pulsed electrical discharge through an $\sim 2\%$

---

mixture of CH_2F_2 (Aldrich, 99.9%) in argon that was premixed in a stainless-steel cylinder. The typical backing pressure was ~1 bar. The discharge was initiated by an 800 V pulse with a duration of $10-50$ μs, with a current-limiting 10 kΩ ballast resistor. The timing of the laser, nozzle, and discharge firing was controlled by a digital delay generator (Stanford Research Systems, model DG535), which also generated a variable-width gate pulse for the high-voltage pulser (Directed Energy, model GRX-1.5K-E). The laser system consisted of an Etalon narrowed dye laser (Lambda-Physik Scanmate 2E) operating on Coumarin 307 dye, pumped by the second or third harmonic of an injection seeded Nd:YAG laser (Continuum Powerlite 7010). For access to wavelengths of <430 nm, the fundamental dye output was mixed with the Nd:YAG fundamental in a BBO crystal. The laser beam was not focused, and typical pulse energies were ~500 μJ in a ~3-mm-diameter beam. A quartz window was used to direct a portion of the dye laser fundamental into an Fe$-$Ne or Fe$-$Ar lamp for absolute wavelength calibration using the optogalvanic effect. When the frequency mixing scheme was used, the Nd:YAG fundamental frequency (9397.44 cm^{-1}) was determined by optogalvanic measurement of both the dye fundamental and sum frequency.

These measurements utilized a mutually orthogonal geometry of laser, molecular beam, and detector, where the laser beam crossed the molecular beam at a distance of ~10 mm downstream. Fluorescence was collected by a two-lens (f/2.4) condenser assembly and filtered via an appropriate long-pass cutoff filter (Corion) prior to striking a photomultiplier tube detector (Oriel) held at a potential of typically -600 V. In acquiring fluorescence excitation spectra, the photomultiplier tube (PMT) signal was terminated to 15 kΩ and digitized by a fast oscilloscope (Hewlett-Packard model HP 54521A), and a "fast scan" mode was typically used, where 10 laser shots were averaged in the baseline and 30 laser shots on the peaks.

Transition frequencies were determined by fitting isolated lines to a Gaussian line shape function, using a nonlinear least-squares fitting routine in PSIPlot software. The transition frequencies were then fit to a standard asymmetric top Hamiltonian, using a least-squares routine in the AsyrotWin program package of Judge and Clouthier,[39] incorporating the well-known ground-state rotational constants.[28–30,40]

Results and Discussion

Rotational Analysis of the Pure Bending Bands (2_0^n). We obtained and rotationally analyzed fluorescence excitation spectra of the levels 2_0^n with $n = 0-7$. Because the 2_0^1 and 0_0^0 bands were previously measured at room temperature and under higher resolution,[28–30] our work did not improve on the fit parameters. Below, we describe in detail our results for the higher-energy bands.

Figure 1 displays a spectrum of the prominent sub-bands observed in the 2_0^2 transition and a simulation of the $\Delta K = \pm 1$ sub-bands, whereas Figure 2 displays an expanded view of the $K_a' = 1 \leftarrow K_a'' = 0$ sub-band. Scattered perturbations were observed in sub-bands with $K_a' \geq 1$.[34] A total of 39 transitions were included in the fit, and Table 1 lists the determined fit parameters. Our value for the rotational constant A, 32.462(69) cm^{-1}, is consistent with, but more precise than, that of Schmidt et al.,[33] who estimated A from the $^qQ_0-^rQ_0$ separation. This method works well for the lower-energy bands[34] but is unreliable at higher energies, where the strong RT interaction typically leads to a splitting of the $K_a' = 1 \leftarrow K_a'' = 0$ sub-band.[34,35]
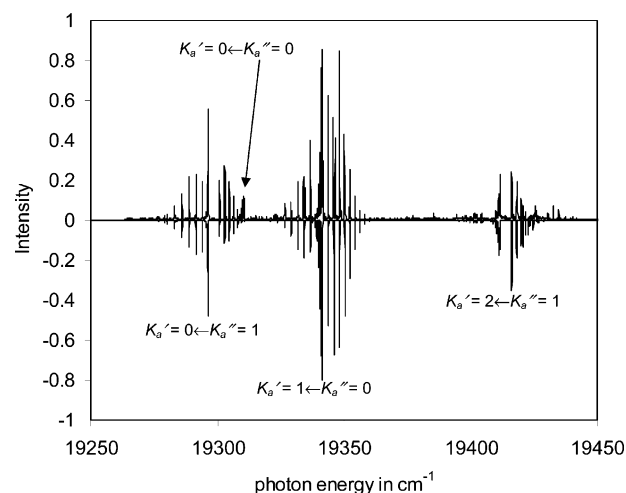

Figure 1. Experimental (top) and simulated fluorescence excitation spectrum of the 2_0^2 band. The sub-band assignments are marked, and the rotational temperature is 20 K.
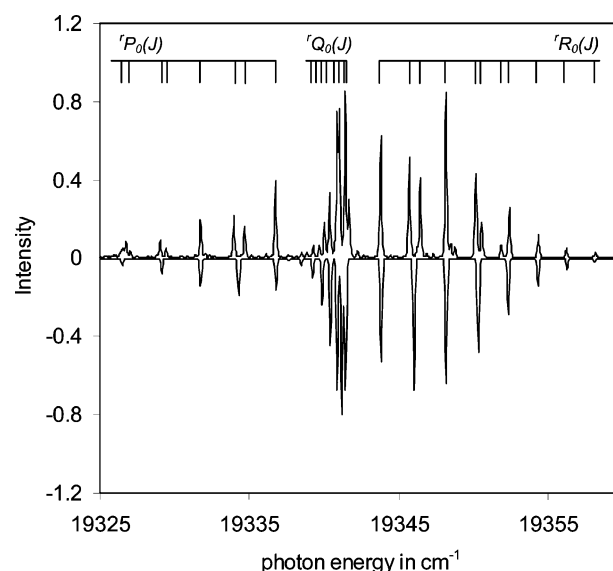

Figure 2. Expanded view of the spectrum in Figure 1, showing the region of the $K_a' = 1 \leftarrow K_a'' = 0$ sub-band. Rotational assignments and perturbation patterns are indicated, and the experimental spectrum lies at the top.

The well-resolved $^rP_0$ and $^rR_0$ branches of the $K_a' = 1 \leftarrow K_a'' = 0$ sub-band reveal obvious perturbations that affected the upper-state levels 2_{11}, 4_{13}, and 5_{14} (see Figure 2), each of which is apparently perturbed by a single background level. Using the formulas that result from two-level perturbation theory, under the assumption that 2_0^2 carries all of the oscillator strength, and incorporating the predicted positions for these levels determined from the global fit, we derive coupling matrix elements of 0.36, 0.18, and 0.22 cm^{-1}, respectively, for these levels.

We conducted Zeeman quantum beat experiments to aid in identifying the perturbing level(s), the full details of which will be given elsewhere. As discussed by Hirota and co-workers,[31–33] the Zeeman effect in the $\tilde{A}$ state can result from the RT interaction with high-lying levels of $\tilde{X}^1A''$ and/or spin$-$orbit interaction with levels of $\tilde{a}^3A''$. Their analysis of apparently unperturbed transitions in the 0_0^0 band revealed excited-state Landé g-factors (g_{aa}) of ~0.005$-$0.010.[33] However, some perturbed lines exhibited much larger Zeeman effects, up to $1.0\mu_B$, which were attributed to singlet$-$triplet interactions.[31]

TABLE 1: Fit Parameters for the HCF(Ã¹A″) Bands Measured in This Work[a]

band	T (cm⁻¹)	A (cm⁻¹)	$(B+C)/2$ (cm⁻¹)	$(B-C)/2$ (cm⁻¹)	Δ_K	N[b]	σ[c]
0_0^0	17282.027(16)	25.686(8)	1.1337(12)	0.0296(12)	0.0434(9)	57	0.019
2_0^1	18303.848(74)	29.606(32)	1.1324(20)		0.144(3)	52	0.073
3_0^1	18551.784(63)	25.80(12)	1.1267(70)	0.0171(70)	0.090(29)	36	0.050
2_0^2	19313.785(37)	32.462(69)	1.1328(29)	0.0238(29)	0.624(17)	39	0.039
$2_0^1 3_0^1$	19567.057(68)	29.05(10)	1.1215(38)	0.0322(38)	0.183(23)	49	0.067
2_0^3	20305.737(60)	38.919(89)	1.1337(32)	0.0299(32)	0.918(21)	39	0.057
$2_0^2 3_0^1$	20562.330(62)	35.54(9)	1.1180(33)	0.0294(33)	0.646(22)	44	0.066
$1_0^1 2_0^1$	21051.100(51)	26.445(72)	1.1302(30)	0.0319(30)	0.114(17)	36	0.049
2_0^4	21279.326(37)	51.8(5)	1.1290(18)		1.16[d]	13	0.028
$2_0^3 3_0^1$	21545.38(13)	41.12(22)	1.1216(52)		0.433(52)	36	0.11
$1_0^1 2_0^2$	22024.298(82)	29.94(12)	1.1291(71)	0.0400(71)	0.175(28)	27	0.069
2_0^5	22242.795(32)	72.5(5)	1.1316(12)		1.50[d]	14	0.028
$1_0^1 2_0^3$	22981.395(77)	37.32(14)	1.129(11)	0.023(11)	0.785(33)	32	0.056
2_0^6	23196.83(20)	126.73(33)	1.132(22)		5.05(7)	27	0.16
$1_0^1 2_0^4$	23922.661(69)	49.87(2)	1.1300(31)		1.16[d]	20	0.052
2_0^7	24150.225(53)		1.1345(27)			12	0.039
$1_0^1 2_0^5$	24847.116(60)		1.1283(31)			10	0.041
$1_0^1 2_0^6$	25757.800(70)		1.1303(36)			9	0.047

[a] Three standard errors given in parentheses. [b] Number of transitions included in the fit. [c] Standard deviation of the fit. [d] Fixed in the fit.
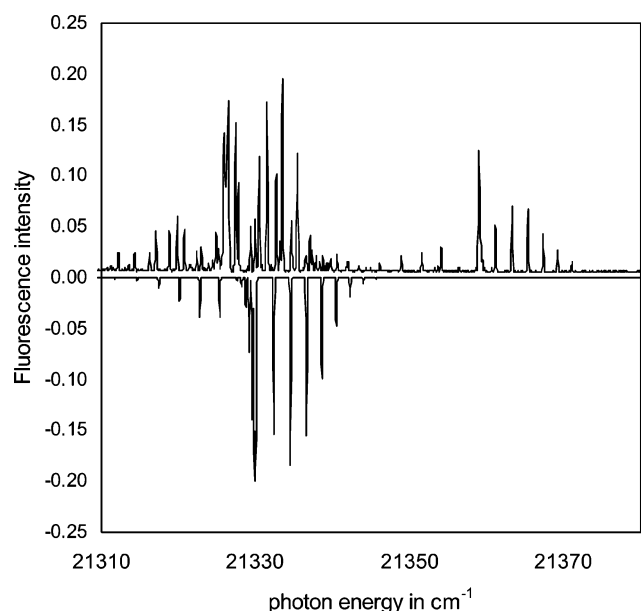

Figure 3. Experimental (top) and simulated fluorescence excitation spectrum of the 2_0^4 band, showing the region of the $K_a' = 1 \leftarrow K_a'' = 0$ sub-band.

The two components of $^rR_0(1)$ transition of 2_0^2 display Landé g-factors of 0.406(10) and 0.267(5), which is consistent with the Ã¹A″− ã³A″ interaction.

For the 2_0^3 band, we again find that all sub-bands with $K_a' \geq 1$ show some perturbations. As previously discussed, transitions were assigned using combination differences, and any perturbed levels were excluded from the fit, which included a total of 39 transitions (see Table 1). The derived A value is 38.919(89) cm⁻¹, revealing the expected increase with bending excitation.[34,35]

For all levels above 2^3, sub-bands with $K_a' \geq 1$ are severely perturbed. To illustrate, Figure 3 displays the region of the $K_a' = 1 \leftarrow K_a'' = 0$ sub-band of 2_0^4, which actually consists of two sub-bands, one of which is severely rotationally perturbed. The higher-energy band can be conclusively identified as a second $K_a' = 1 \leftarrow K_a'' = 0$ sub-band and not the $2_0^4 3_1^1$ sequence band as previously suggested,[34] for the following reasons. First, we have not observed hot bands anywhere in

our spectra. Second, we do not observe any of the other sub-bands expected for the $2_0^4 3_1^1$ transition. Third, if we assume an A constant similar to that (derived below) for 2_0^4, a fit of this sub-band yields a vibronic origin of 20 311.865(42) cm⁻¹, which is only 32 cm⁻¹ above the origin of 2_0^4. This band should occur ~115 cm⁻¹ higher, based on the position of $2^4 3^1$ predicted from our vibrational analysis (see below) and the reported ground-state C−F stretching frequency.[41] We therefore conclude that the two sub-bands result from the (perturbed) $K_a' = 1$ level of 2_0^4, and the large splitting implicates the RT interaction. Support for this hypothesis comes in the drastically lengthened fluorescence lifetimes for these sub-bands compared to that for the $K_a' = 0$ level of 2_0^4,[35] and in the hyperfine structure determined from our polarization QBS measurements,[36] which reveals very small ¹⁹F and ¹H hyperfine constants for the higher-energy sub-band (upper panel of Figure 4), diagnostic of the RT interaction.[36]

Following the pattern of the lower-energy bands, the $K_a' = 0 \leftarrow K_a'' = 1$ sub-band of 2_0^4 was unperturbed,[35] and a fit of this sub-band yielded the band origin and effective rotational constant (see Table 1). To determine the value of A, we included in the fit two unperturbed transitions in the $K_a' = 2 \leftarrow K_a'' = 1$ sub-band and fixed the centrifugal distortion term Δ_K at 1.16 cm⁻¹, which is a value obtained from a linear extrapolation of the constants for the lower-energy bands. The fit yielded $A = 51.8(5)$ cm⁻¹ (see Table 1). We emphasize that the $K_a' = 2 \leftarrow K_a'' = 1$ sub-band was also extensively rotationally perturbed but was not split in the manner of the $K_a' = 1 \leftarrow K_a'' = 0$ sub-band.

Turning to the lower-energy $K_a' = 1 \leftarrow K_a'' = 0$ sub-band in 2_0^4, we assigned splitting patterns in the $^rP_0$ and $^rR_0$ branches using ground-state combination differences. Every upper-state level is perturbed; however, the 3_{12}, 4_{13}, and 5_{14} levels each appear to be perturbed by a single background level. Following the procedure described previously, we derive coupling matrix elements of 0.50, 0.37, and 0.31 cm⁻¹, respectively. Again, the large Zeeman effect and ¹⁹F and ¹H hyperfine constants observed for transitions in the lower-energy sub-band (Figure 4) implicate spin−orbit mixing with levels of the ã³A″ state.

The pattern of the $K_a' = 1 \leftarrow K_a'' = 0$ sub-band in 2_0^4 is reminiscent of a "doorway" model, similar to that used to model rovibrational interactions in the ground electronic manifold of
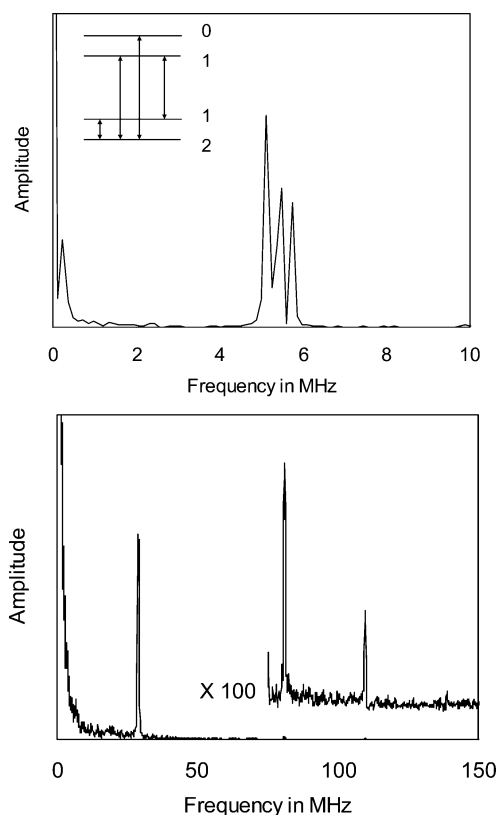
Figure 4. (Upper panel) Zero-field polarization quantum beat spectrum for the $^rR_0(1)$ transition in the higher-energy $K_a' = 1 \leftarrow K_a'' = 0$ sub-band of 2_0^4. (Lower panel) Similar spectrum for the lowest-energy component of the perturbed $^rR_0(1)$ transition in the lower-energy $K_a' = 1 \leftarrow K_a'' = 0$ sub-band.

a variety of polyatomic molecules over the past decade.[42–45] Typically, in this model a bright state is coupled to a "doorway" state by a large (low-order) interaction, which, in turn, is coupled to a bath of background states via higher-order interactions.[42,43] Here, of course, the former is the RT interaction, and the latter spin−orbit (or Coriolis) interaction. It may seem unusual that only the lower-energy member of the RT pair is affected by the latter; however, the triplet level density is sparse. We emphasize that our use of the term "doorway" does not imply the existence of a unique state that facilitates the $\tilde{A}^1A''-\tilde{a}^3A''$ interaction: we have no evidence of this.

The overall structure of the 2_0^5 band is similar to that of 2_0^4, in that two sub-bands are apparently observed in the region of the $K_a' = 1 \leftarrow K_a'' = 0$ sub-band, shown in Figure 5. However, each band is severely rotationally perturbed, and, because of band overlap, it was not possible to assign the perturbed lines using combination differences. A tentative assignment of the higher-energy sub-band to the $2_0^5 3_1^1$ sequence band[34] can be eliminated for the previously mentioned reasons. A fit of the $K_a' = 0 \leftarrow K_a'' = 1$ sub-band yielded the band origin and effective rotational constant $B = \frac{1}{2}(B + C)$, and the parameters are given in Table 1. To determine the value of the constant A, we included in the fit two unperturbed transitions in the $K_a' = 2 \leftarrow K_a'' = 1$ sub-band, which, again, was severely rotationally perturbed but not split in the manner of the $K_a' = 1 \leftarrow K_a'' = 0$ sub-band. The centrifugal distortion term Δ_K was fixed at 1.45 cm^{-1} in the fit, which yielded $A = 72.5(5)$ cm^{-1}.

We identified several unperturbed transitions in the $K_a' = 2 \leftarrow K_a'' = 1$ and $K_a' = 0 \leftarrow K_a'' = 1$ sub-bands of 2_0^6, whereas, again, two weak and heavily perturbed $K_a' = 1 \leftarrow K_a'' = 0$ sub-bands were observed. A total of 27 transitions were included
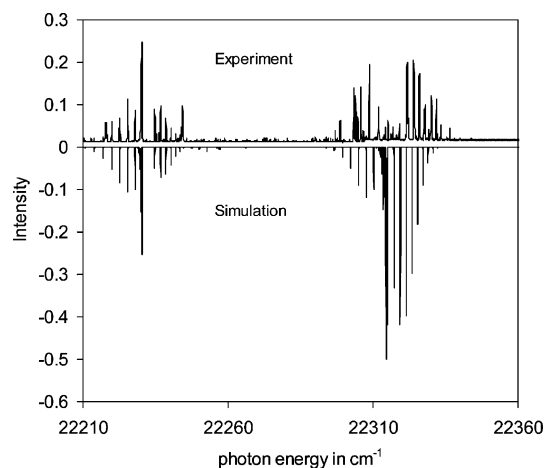

Figure 5. Experimental (top) and simulated fluorescence excitation spectrum of 2_0^5, showing the region of the $K_a' = 0 \leftarrow K_a'' = 1$ and $K_a' = 1 \leftarrow K_a'' = 0$ sub-bands.
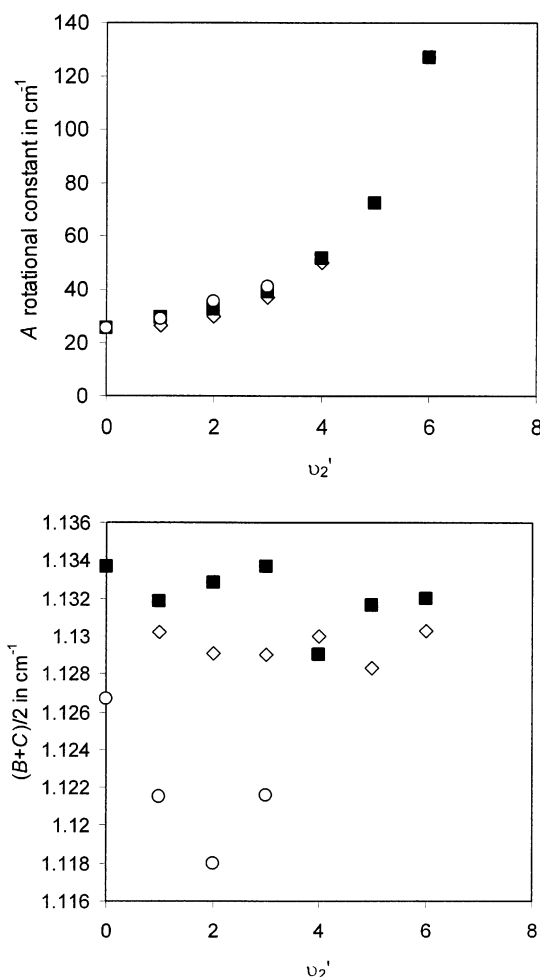

Figure 6. Dependence of the rotational constants A (upper panel) and B_{eff} ($B_{\text{eff}} = (B + C)/2$) on quanta of bending excitation for the measured bands. Legend: (■) $(0,v_2',0)$, (◇) $(1,v_2',0)$, and (○) $(0,v_2',1)$.

in the fit (see Table 1). For 2_0^7, we were only able to rotationally analyze the $K_a' = 0 \leftarrow K_a'' = 1$ sub-band, and Table 1 lists the determined band origin and effective rotational constant.

The dependence of the rotational constants A and $B_{\text{eff}} = (B + C)/2$ on bending quanta are shown in the upper and lower panels, respectively, of Figure 6. Note in particular the dramatic increase in A with increasing bending excitation, initially

reported by Kable and co-workers,[34] which signals the approach to linearity.[35] In contrast, B_{eff} displays a weak dependence on the quanta of bend for the pure bending levels.

Rotational Analysis of $2_0^n 3_0^1$ Bands. Approximately 250 cm^{-1} above 2_0^1, we found a series of weaker, unperturbed sub-bands clearly associated with a single vibronic level. At least two of these sub-bands were previously observed and assigned to hot-band transitions.[34] We assign these as sub-bands of the 3_0^1 transition, based on the following evidence. First, the derived constant A (25.79(12) cm^{-1}) is similar to that of 2^0 but significantly smaller than that of 2^1, indicating that the bending mode is not excited. Second, the derived B and C constants (see Table 1) are smaller than those of 2^0 or 2^1, which is consistent with excitation of the C$-$F stretch. Finally, the position of this band is consistent with the predicted Ã-state C$-$F stretching frequency.[26] A total of 35 transitions were included in the fit (see Table 1).

We subsequently recorded and rotationally analyzed spectra for other members of the relatively weak $2_0^n 3_0^1$ progression, spanning $n = 1-3$. The derived spectroscopic constants are listed in Table 1. In all cases, the rotational constant A closely follows that of the corresponding member of the 2_0^n progression, as shown in Figure 6. As expected, the effective rotational constants $B_{eff} = (B + C)/2$ are noticeably smaller than those of the 2_0^n progression (see Figure 6).

Rotational Analysis of $1_0^1 2_0^n$ Bands. Nauta et al.[46] recently reported the band origins and A rotational constants of a new series of bands in this system, assigned to the $1_0^1 2_0^n$ progression. Bands with $n = 1-4$ were observed, and the assignments were confirmed via dispersed fluorescence spectroscopy.[46] With this information in hand, we observed and rotationally analyzed the series of bands $1_0^1 2_0^n$ with $n = 1-6$, and the fit parameters are given in Table 1. The derived values of A closely follow those of the 2_0^n progression, whereas the effective rotational constants $B_{eff} = (B + C)/2$ are slightly smaller (see Figure 6).

The $1^1 2^6$ level lies above the dissociation asymptote to CF($^2\Pi$) + H(^{2}S), which is calculated to lie ~7350 cm^{-1} above the vibrationless level with a barrier to dissociation of ~1605 cm^{-1}.[26] Using the A constant determined in this work for 2^6, the $K_a' = 1$ level of $1^1 2^6$ is predicted to lie ~353 cm^{-1} below the barrier, whereas the $K_a' = 2$ level should lie ~25 cm^{-1} *above* it. Indeed, we found a very weak and strongly perturbed $K_a' = 1$ sub-band near 25 837 cm^{-1}. This level showed no evidence of a reduced fluorescence lifetime, placing a lower limit on the barrier to dissociation in the Ã^{1}A$''$ state of ~8555 cm^{-1} above the vibrationless level. Despite repeated attempts, we were unable to observe the $1^1 2^7$ level by laser-induced fluorescence.

Vibrational Analysis. As shown in Table 2, where they can be compared, the anharmonic Ã-state vibrational frequencies determined in this work are in good agreement with the predictions of a recent theoretical study.[26] Moreover, the observed vibrational spacings for the pure bending levels 2^n show the expected linear dependence on the quanta of bending excitation up to 2^5, as shown in the upper panel of Figure 7. Several studies have examined the vibrational levels of a nonlinear molecule near and above the barrier to linearity.[47-49] Dixon[48] showed that the bending vibrational intervals reach a minimum at the barrier and increase above it; therefore, a plot of the vibrational intervals versus the mean vibronic energy exhibits a minimum ("Dixon dip") at the barrier.[48] Such a plot is shown for our data in the lower panel of Figure 7, and a minimum is clearly observed around the 2^7 level. To estimate the barrier height, we fit the intervals for $v_2' = 2-7$ to a quadratic function,[48] as shown in Figure 7. The minimum

TABLE 2: Derived HCF(Ã^{1}A$''$) Vibrational Energies and Theoretical Predictions

	Vibrational Energy (cm^{-1})	
level[a]	experimental[b]	range of theoretical predictions[c]
(0,0,0)	0	
(0,1,0)	1021.8	1006.6−1037.7
(0,0,1)	1269.8	1259.6−1260.1
(0,2,0)	2031.8	1996.6−2060.0
(0,1,1)	2285.0	2257.4−2291.1
(0,3,0)	3023.7	2967.4−3064.2
(0,2,1)	3280.3	
(1,1,0)	3769.1	3673.4−3827.8
(0,4,0)	3997.3	3915.6−4047.4
(0,3,1)	4263.4	
(1,2,0)	4742.3	
(0,5,0)	4960.8	4835.8−5006.0
(1,3,0)	5699.4	
(0,6,0)	5914.9	5719.8−5935.3
(1,4,0)	6640.6	
(0,7,0)	6868.2	6564.5−6834.9
(1,5,0)	7565.1	
(1,6,0)	8475.8	

[a] Notation (v_1,v_2,v_3), where v_1 is the C$-$H stretch, v_2 is the bend, and v_3 is the C$-$F stretch. [b] Uncertainty of ±0.1 cm^{-1}. [c] From ref 26.
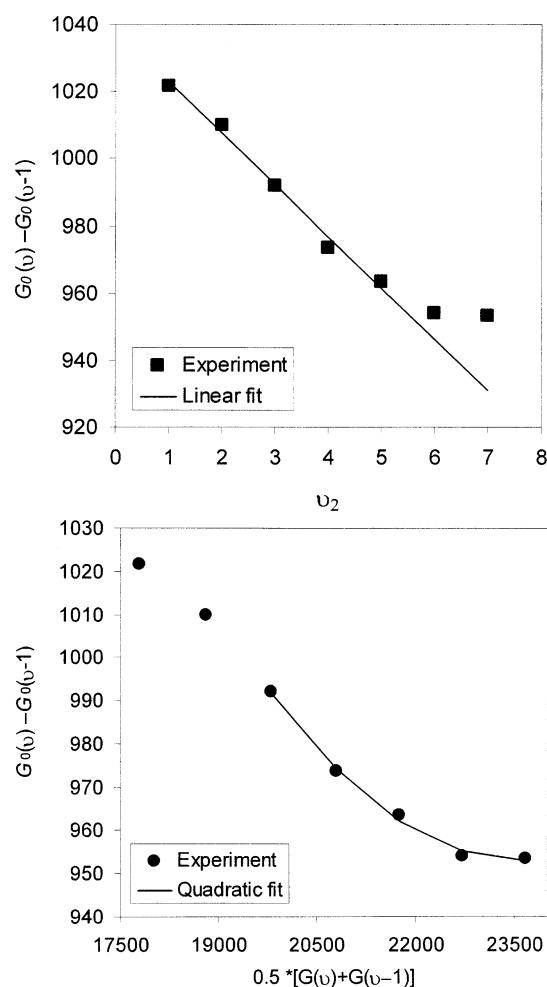

Figure 7. Plot of the vibrational intervals for the pure bending states $(0,v_2',0)$ versus quanta of bending excitation (upper panel) and average vibronic energy (lower panel). A linear fit of the data up to (0,5,0) is shown in the upper panel, whereas the lower panel displays a quadratic fit to the data near the minimum.

determined from this fit gives a barrier height of 6300 ± 270 cm^{-1} above the vibrationless level, which may be compared with the (zero-point-corrected) theoretical estimate of 6777 cm^{-1}.[26]

Electronic Spectroscopy of HCF($\tilde{A}^1A'' \leftarrow \tilde{X}^1A'$)

J. Phys. Chem. A, Vol. 108, No. 17, 2004 **3737**

TABLE 3: Derived HCF($\tilde{A}^1A''$) Vibrational Parameters and Theoretical Predictions

parameter	this work (cm^{-1})	range of theoretical predictions (cm^{-1})[a]
ω_1^0	2784.9(24)[b]	2697−2828[c]
ω_2^0	1029.9(8)	1035−1041
ω_3^0	1270.8(17)[b]	1259.6−1260.1[c]
x_{12}^0	−36.6(6)	
x_{22}^0	−7.5(2)	
x_{23}^0	−10.0(10)	

[a] Anharmonic frequency. [b] From ref 26. [c] Fundamental frequency.

The vibrational frequencies, excluding 2^7, were fit using a nonlinear least squares routine to a standard anharmonic potential function of the form[50]

$$G_0(v_1, v_2, v_3) = \omega_1^0 v_1 + \omega_2^0 v_2 + \omega_3^0 v_3 + x_{22}^0(v_2)^2 + x_{12}^0 v_1 v_2 + x_{23}^0 v_2 v_3 \quad (1)$$

where ω_i^0 is the frequency of mode i, x_{ii}^0 a diagonal anharmonicity constant, and x_{ij}^0 a cross-anharmonicity constant. Only levels with single quanta of excitation in v_1 and v_3 were observed; therefore, the corresponding diagonal anharmonicity constants could not be determined, and the derived frequencies represent anharmonic values. The fit incorporated 16 vibrational levels and yielded a standard deviation of 2.1 cm^{-1}. The fit parameter values are compared in Table 3 with available theoretical predictions.[26]

Conclusions

We recorded and rotationally analyzed fluorescence excitation spectra of the pure bending transitions 2_0^n with $n = 0-7$ and the combination bands $1_0^1 2_0^n$ with $n = 1-6$ and $2_0^n 3_0^1$ with $n = 0-3$ in the HCF $\tilde{A}^1A'' \leftarrow \tilde{X}^1A'$ system. (A tabular display of the observed and calculated line positions of the HCF $\tilde{A}^1A'' \leftarrow \tilde{X}^1A'$ system is given in the Supporting Information.) Spectra of the $2_0^n 3_0^1$ bands are reported here for the first time, and our analysis has yielded precise new values for the $\tilde{A}$-state vibrational frequencies and rotational constants. The approach to linearity in the $\tilde{A}$-state is evidenced in the sharp increase in the rotational constant A with increasing bending excitation, as first reported by Kable and co-workers, and a minimum in the vibrational intervals near the 2^7 level. A quadratic fit to the vibrational intervals of the pure bending levels gives a barrier to linearity of 6300 ± 270 cm^{-1} above the vibrationless level. Our observation of the $K_a' = 1$ level of $1^1 2^6$ places a lower limit on the barrier to dissociation in the $\tilde{A}$-state of ~ 8555 cm^{-1} above the vibrationless level. Where they can be compared, the derived $\tilde{A}$-state parameters are in excellent agreement with the predictions of ab initio electronic structure theory.

Numerous perturbations were observed in sub-bands with $K_a' \geq 1$, particularly at higher energies, reflecting interactions with background levels of both the $\tilde{X}^1A''$ and $\tilde{a}^3A''$ states. These interactions can be differentiated on the basis of Zeeman and hyperfine measurements,[36] and the analysis of perturbations in this system will be the subject of future work.

Supporting Information Available: Table of observed and calculated line positions (PDF). This material is available free of charge via the Internet at http://pubs.acs.org.

References and Notes

(1) Moss, R. A., Jones, M., Jr., Eds. *Carbenes*; Reactive Intermediates in Organic Chemistry Series; Wiley−Interscience: New York, 1973; Vol. I. (b) Moss, R. A., Jones, M., Jr., Eds. *Carbenes*, Vol. II; Reactive Intermediates in Organic Chemistry Series; Wiley−Interscience: New York, 1975; Vol. II.

(2) Kirmse, W. *Carbene Chemistry*, 2nd Ed.; Academic Press: New York, 1971.

(3) Sciano, J. C. In *Handbook of Organic Photochemistry*; CRC Press: Boca Raton, FL, 1989; Vol. 2, Chapter 9.

(4) Carey, F. A.; Sundberg, R. J. In *Advanced Organic Chemistry, Part 3*, 3rd ed.; Plenum Press: New York, 1990.

(5) Weirsum, U. E.; Jenneskens, L. W. In *Gas-Phase Reactions in Organic Synthesis*; Vallée, Y., Ed.; Gordon and Breach; Amsterdam, 1997; p 143.

(6) Dean, A. M.; Bozzelli, J. W. In *Gas-Phase Combustion Chemistry*; Gardiner, W. C., Jr., Ed.; Springer; New York, 2000; Chapter 2.

(7) Bacskay, G. B.; Martoprawiro, M.; Mackie, J. C. *Chem. Phys. Lett.* **1998**, *290*, 391.

(8) Sendt, K.; Ikeda, E.; Bacskay, G. B.; Mackie, J. C. *J. Phys. Chem. A* **1999**, *103*, 1054.

(9) Martoprawiro, M.; Bacskay, G. B.; Mackie, J. C. *J. Phys. Chem. A* **1999**, *103*, 3923.

(10) Sendt, K.; Bacskay, G. B.; Mackie, J. C. *J. Phys. Chem. A* **2000**, *104*, 1861.

(11) Wayne, R. P. *Chemistry of Atmospheres*, Oxford University; Oxford, U.K., 1991; Chapter 8 and references therein.

(12) Carter, E. A.; Goddard, W. A., III. *J. Chem. Phys.* **1998**, *88*, 1752.

(13) Bauschlicher, C. W., Jr.; Schaefer, H. F., III; Bagus, P. S. *J. Am. Chem. Soc.* **1977**, *99*, 7106.

(14) Koda, S. *Chem. Phys. Lett.* **1978**, *55*, 353.

(15) Bauschlicher, C. W., Jr. *J. Am. Chem. Soc.* **1980**, *102*, 5492.

(16) Scseria, G. E.; Durán, M.; Maclagan, R. G. A. R.; Schaefer, H. F., III. *J. Am. Chem. Soc.* **1986**, *108*, 3248.

(17) Irikura, K. K.; Goddard, W. A., III; Beauchamp, J. L. *J. Am. Chem. Soc.* **1999**, *114*, 48.

(18) Carter, E. A.; Goddard, W. A., III. *J. Phys. Chem.* **1987**, *91*, 4651.

(19) Shin, S. K.; Goddard, W. A., III; Beauchamp, J. L. *J. Phys. Chem.* **1990**, *94*, 6963.

(20) Shin, S. K.; Goddard, W. A., III; Beauchamp, J. L. *J. Chem. Phys.* **1990**, *93*, 4986.

(21) Gutsev, G. L.; Ziegler, T. *J. Phys. Chem.* **1991**, *95*, 7220.

(22) Russo, N.; Sicilia, E.; Toscano, M. *J. Chem. Phys.* **1992**, *97*, 5031.

(23) Gobbi, A.; Frenking, G. *J. Chem. Soc. Chem. Commun.* **1993**, 1162−1164.

(24) Garcia, V. M.; Castell, O.; Reguero, M.; Callol, R. *Mol. Phys.* **1996**, *87*, 1395.

(25) Weis, B.; Rosmus, P.; Yamashita, K.; Morokuma, K. *J. Chem. Phys.* **1990**, *92*, 6635.

(26) Schmidt, T. W.; Bacskay, G. B.; Kable, S. H. *Chem. Phys. Lett.* **1998**, *292*, 80.

(27) Patel, R. I.; Stewart, G. W.; Casleton, K.; Gole, J. L.; Lombardi, J. R. *Chem. Phys.* **1980**, *52*, 461.

(28) Merer, A. J.; Travis, D. N. *Can. J. Phys.* **1966**, *44*, 1541.

(29) Kakimoto, M.; Saito, S.; Hirota, E. *J. Mol. Spectrosc.* **1981**, *88*, 300.

(30) Suzuki, T.; Saito, S.; Hirota, E. *J. Mol. Spectrosc.* **1981**, *90*, 447.

(31) Butcher, R. J.; Saito, S.; Hirota, E. *J. Chem. Phys.* **1984**, *80*, 4000.

(32) Suzuki, T.; Saito, S.; Hirota, E. *Can. J. Phys.* **1984**, *62*, 1328.

(33) Suzuki, T.; Hirota, E. *J. Chem. Phys.* **1986**, *85*, 5541.

(34) Schmidt, T. W.; Bacskay, G. B.; Kable, S. H. *J. Chem. Phys.* **1999**, *110*, 11277.

(35) Fan, H.; Ionescu, I.; Annesley, C.; Reid, S. A. *Chem. Phys. Lett.* **2003**, *378*, 548.

(36) Ionescu, I.; Fan, H.; Annesley, C.; Xin, J.; Reid, S. A. *J. Chem. Phys.* **2004**, *120*, 1164.

(37) Xin, J.; Fan, H.; Ionescu, I.; Annesley, C.; Reid, S. A. *J. Mol. Spectrosc.* **2003**, *219*, 37.

(38) Xin, J.; Ionescu, I.; Kuffel, D.; Reid, S. A. *Chem. Phys.* **2003**, *291*, 61.

(39) Judge, R. H.; Clouthier, D. J. *Comput. Phys. Commun.* **2001**, *135*, 293.

(40) Wagner, M.; Gamperling, M.; Braun, D.; Prohaska, M.; Hütter, W. *J. Mol. Struct.* **2000**, *517−518*, 327.

Fan et al.

(41) Suzuki, T.; Hirota, E. *J. Chem. Phys.* **1988**, *88*, 6778.

(42) Go, J.; Perry, D. S. *J. Chem. Phys.* **1992**, *97*, 6994.

(43) McIlroy, A.; Nesbitt, D. J.; Kerstel, E. R. Th.; Pate, B. H.; Lehmann, K. K.; Scoles, G. *J. Chem. Phys.* **1994**, *100*, 2596.

(44) Cupp, S.; Lee, C. Y.; McWhorter, D.; Pate, B. H. *J. Chem. Phys.* **1998**, *109*, 4302.

(45) Boyarkin, O. V.; Rizzo, T. R.; Perry, D. S. *J. Chem. Phys.* **1999**, *110*, 11346.

(46) Nauta, K.; Guss, J. S.; Owens, N. L.; Kable, S. H. *J. Chem. Phys.* **2004**, *120*, 3517.

(47) Thorson, W. R.; Nakagawa, I. *J. Chem. Phys.* **1960**, *33*, 994.

(48) Dixon, R. N. *Trans. Faraday Soc.* **1964**, *60*, 1363.

(49) Merer, A. J.; Travis, D. N. *Can. J. Phys.* **1966**, *44*, 525.

(50) Herzberg, G. *Molecular Spectra and Molecular Structure III. Electronic Spectra of Polyatomic Molecules*; Van Nostrand: New York, 1966.